Arabian Journal of Chemistry (2020) 13, 6802–6814

King Saud University

Arabian Journal of Chemistry

www.ksu.edu.sa
www.sciencedirect.com

ORIGINAL ARTICLE

Green synthesis of Copper oxide nanoparticles decorated with graphene oxide for anticancer activity and catalytic applications

Kavitha Ganesan [a], Vinoth Kumar Jothi [a], Abirami Natarajan [a,*], Arulmozhi Rajaram [a], Siranjeevi Ravichandran [a], Satish Ramalingam [b]

[a] *Department of Chemistry, Faculty of Enginereeing and Technology, SRM Institute of Science and Technology, Kattankulathur, Tamil Nadu-603 203, India*
[b] *Department of Genetic Engineering, School of Bio-Engineering, SRM Institute of Science and Technology, Kattankulathur, Tamil Nadu-603 203, India*

Received 16 April 2020; accepted 23 June 2020
Available online 30 June 2020

KEYWORDS

GO-CuO nanocomposites;
Decolorization;
Cytotoxic activity;
Drug delivery;
Human colon cancer cell

Abstract Nanotechnology is an embryonic field that grips countless impacts on the drug delivery system. Nanoparticles as haulers increase the capability of target-specific drug delivery to many folds hence are used in the treatment of dreadful diseases such as cancer, diabetes, etc. This boom has aimed at, to synthesize Copper oxide nanoparticles (CuO-NPs) using *Acalypha Indica* leaf extract and then incorporated with graphene oxide (GO) to form GO-CuO nanocomposites. Secondly, to sightsee the photocatalytic activity of CuO-NPs and GO-CuO nanocomposites towards the decolorization of methylene blue-dye and to test its activity against HCT-116 Human colon cancer cell lines. Synthesized nanocomposites were characterized using FTIR, UV–vis, X-ray powder diffraction (XRD), scanning electron microscopy (SEM), energy dispersive X-ray analysis (EDAX), X-ray Photoelectron Spectroscopy (XPS) and transmission electron microscopy (TEM) analysis. The photocatalytic studies revealed that synthesized nanocomposites have the efficiency to degrade methylene blue dye by 83.20% and cytotoxic activity was found to be 70% against HCT-116 Human colon cancer cell lines at 100 μg/ml. GO-CuO nanocomposites have appreciable activity towards cancer cell lines and photocatalytic activity when compared to nanoparticles as such.
© 2020 The Authors. Published by Elsevier B.V. on behalf of King Saud University. This is an open access article under the CC BY-NC-ND license (http://creativecommons.org/licenses/by-nc-nd/4.0/).

1. Introduction

In recent years, nanomaterials and nanoparticles have generally been used for an assortment of purposes, including, cosmetics, diagnosis, targeted drug delivery, imaging, and biosensor (Ramesh et al., 2014). Nanoparticles are used as a carriage for cellular labels for imaging *in vitro* and *in vivo*.

* Corresponding author.
E-mail address: abiramin@srmist.edu.in (A. Natarajan).
Peer review under responsibility of King Saud University.

ELSEVIER Production and hosting by Elsevier

https://doi.org/10.1016/j.arabjc.2020.06.033
1878-5352 © 2020 The Authors. Published by Elsevier B.V. on behalf of King Saud University.
This is an open access article under the CC BY-NC-ND license (http://creativecommons.org/licenses/by-nc-nd/4.0/).

Nanoparticles are being studied in photodynamic therapy 12 and the treatment of tumor hyperthermia (Sankar et al., 2013). Nowadays, biosynthesis plays an important part in the preparation of metal oxide nanoparticles. It eliminates toxic chemicals produced by chemical reactions and removes the organic solvent from synthetic protocols. Current research results reveal that plant-derived metal nanoparticles are safe, reliable, and eco-friendly correlated to physical and chemical systems. Plant-mediated nanoparticle synthesis is an inexpensive method and therefore an upcoming profitable alternative for large-scale production (Bansal et al., 2012; Kannan and Sundrarajan, 2015). Plants are known to comprise various therapeutic compounds that have been demoralized as a traditional remedy then ancient times. Its large diversity of plants continues to be explored for a comprehensive series of applications in the fields of medicine, agriculture, and industry and hence used as assets for the production of different nanoparticles.

Recent reports have shown that bioactive compounds such as phenols, alkaloids, terpenoids flavonoids, quinines, tannins, etc., present in plants act as good reducing agents in the synthesis of nanoparticles (Chandrasekaran (2013)). Biological method using aqueous extract of *Thymus vulgaris L.* leaves act as a capping and reducing agent (Nasrollahzadeh et al., 2016). The Rosa canina fruit extract act as a capping agent and reducing agent for the synthesis of CuO NPs (Hekmati, 2019). The aqueous leaves extract of *Thymbra spicata* act as a stabilizing and reducing agent for the synthesis of CuO NPs (Veisi et al., 2017) *Acalypha indica* (Family: Euphorbiaceae), a source of bio-reductants and stabilizers has been reported to be beneficial in treating rheumatism, asthma, pneumonia, and many other diseases (Kavitha et al., 2013). *Acalypha Indica* leaves are used in India's traditional medicine as a jaundice remedy (Sulaiman et al., 2013). *Acalypha Indica* has antibacterial activity against human pathogens causing nosocomial infection (Murugan and Saranraj, 2011; Ishak et al., 2013; Rajaselvam et al., 2012). Acaricides are used both in agriculture and medicine. *Acalypha indica* is a natural diuretic agent (Das et al., 2005). In medicine, diuretics are used to treat liver cirrhosis, heart failure, water poisoning, hypertension, and certain kidney diseases. This herb has anticancerous activity against several types of cancers (Sanseera et al., 2012; Reddy et al., 2012). Other properties of the herb include anti-helminthic (Chengaiah et al., 2009), anti-inflammatory (Shivkar and Kumar, 2003), neuro-protective, anti-fungal (Alade and Irobi, 1993) and anti-oxidant (Prasad and Estari, 2014). Several reports on phyto-assisted synthesis of CuO NPs by different parts of plant extracts have been published including *Aloe vera* (Kerour et al., 2018), *abutilon Indicum* leaf (Ijaz et al., 2017), *Aglaia elaeagnoidea* flower (Manjari et al., 2017), *Camellia japonica* (Maruthupandy et al., 2017), *green pea* (Ochoa et al., 2017) *Saraca indica* leaves (Prasad et al., 2017), *Piper betle* (Praburaman et al., 2016), *Malus Domestica* leaf (Jadhav et al., 2018), and. *Rheum palmatum L.* (Bordbar et al., 2017), *Carica papaya* (Sankar et al., 2014) *Musa acuminate* (Chaudhary et al., 2019). Recently, Copper oxide (CuO) nanoparticles have received considerable curiosity and attention due to their physical and chemical properties. It possess distinct features such as high specific surface area, good electrochemical activity, proper redox potential, and excellent stability in solutions (Khan et al., 2014; Giri and Sarkar, 2016). It is one of the centers of fascination after noble metal nanoparticles. It has auspicious applications in various areas such as sensors/biosensors (Alizadeh and Mirzagholipur, 2014; Annanouch et al., 2015; Nguyen et al., 2018), electrochemistry (Pendashteh et al., 2013; Li et al., 2014; Zampardi et al., 2018), antifouling coatings (Abiraman et al., 2017; Zhao et al., 2017), energy storage (Prasad et al., 2013; Liang et al., 2018), and biocidal agents (Sivaraj et al., 2014; Vaidehi et al., 2018). With the arrival of nanotechnology in biomedical research, enormous development in research activities involving CuO nanoparticles have been prompted. CuO NPs have been broadly used in the non-enzymatic sensing of clinically relevant analytes for the high specific surface area and the prospect of stimulating electron transfer reactions at lower overpotential (Rahimi-Nasrabadi et al., 2013; Xu et al., 2018). CuO nanoparticles have shown their potential in pharmacological activity, specifically in antitumor therapy (Wang et al., 2013; Wu et al., 2018). CuO NPs can act as an efficient catalyst for C—C homocoupling reaction (Sabuj Kanti Das et al., 2020). Cu act as a high-efficiency electrocatalyst for N_2 fixation to NH_3 under ambient conditions (Chengbo Li et al., 2019). Cobalt doped CuO nanoarray was used as an efficient oxygen evolution reaction electrocatalyst with enhanced activity (Xiong et al., 2018).

Presently, the disintegration of synthetic dyes and organic effluents in waste-water employing nanoparticles has attracted researchers to explore in the field of catalysis (Sajan et al., 2016). Amid different photocatalysts, CuO plays an improbable role in the remediation of environmental contaminants and possess certain notable characteristics such as less expensive, safe, efficient, effortlessly, photo-stable available and high photocatalytic performance under solar spectrum that make CuO ideal photocatalytic system (Jiang et al., 2016). However, CuO nanoparticles have only a 2.0 eV bandgap which has the only efficiency of absorption 2–4% in the UV region and its photocatalytic activity is much low (Wei et al., 2017). Another factor which impedes the quantum efficiency is due to profligate recombination of photo-induced electron-hole pairs (Martins et al., 2014). To overcome these limitations, studies have been carried out to enhance CuO photocatalytic activity with a prolonged light-response range and greater quantum efficiency (Almeida et al., 2016). There are numerous methods to amend the physical properties of CuO in order to attain its efficiency level but incorporating with carbonaceous materials such as graphene oxide (GO) in the form of nanocomposites have responded plentiful consideration and these materials possess photostability, large surface area, thermal and high charge mobility and are measured substantial mean to enhance the disintegration activity of CuO (Huang et al., 2018). The nanocomposites results from the combination of GO and CuO have further advantages when compared to CuO NPs as such and it enhances the adsorptive capability of CuO by increasing the surface area (Jiang et al., 2011). Recent reports have shown that CuO NPS and CuO/GO nanocomposite have been amalgamated via microwave irradiation using sugarcane juice. The synthesized CuO/GO NC act as a catalyst (reduction of aromatic nitro compounds), non-enzymatic glucose sensor for food (Shabnam et al., 2017), and an antioxidant (Archita Bhattacharjee et al., 2020). The GO/CuO nanocomposites (NC) were synthesized via sol-gel method plays a vital role in enhancing the wound healing mechanism by cumulative cell proliferation, angiogenesis process, rapid initiation of inflammatory and antimicrobial property (Venkataprasanna

et al., 2020). The GO-CuO which act as photocatalyst for Methyl Red (MR) removal and proficient diesel additive (Sehar et al., 2020). CuO-Graphene Oxide nanocomposite was used for the separation and pre-concentration of polycyclic aromatic hydrocarbons (PAHs) residue in numerous intricate matrices such as fruits, vegetables and actual environmental water samples (Asfaram et al., 2020). GO coated CuO NPs were used for the functionalization of diclofenac and acetylsalicylic acid (Tkach et al., 2020). Cr_2O_3 coated rGO was used for the highly active electrocatalyst for the N_2 reduction at ambient conditions (Xia et al., 2019). CuO@ZnCo-LDH core-shell hetero structured nanowire array on copper foil (CuO@ZnCo LDH/CF)was used as an efficient electrocatalyst for the OER in alkaline media (Wang et al., 2020). P-doped graphene act as an electrocatalyst for N_2 reduction (Tongwei Wu et al., 2020).

The purpose of this exertion is to synthesize CuO oxide nanoparticles using *Acalypha Indica* leaf extract. Further, the nanoparticles were decorated with graphene oxide to produce nanocomposites. Characterization studies, photocatalytic activity on methylene blue, and cytotoxic activity on human colon cancer cell lines were carried out for both synthesized nanoparticles and nanocomposites respectively.

2. Materials and methods

2.1. Materials

The leaves of *Acalypha Indica* were collected in the month of June from Dindigul districts of Tamil Nadu, India. The leaves were confirmed by Dr. M. Ganeshan, Asst. Prof [S.G], IIISM, SRMIST. Copper sulfate, graphite flakes, Sodium Nitrate ($NaNO_3$), Sulphuric acid ($H_2SO_4$98%), potassium permanganate, DMSO (Dimethyl Sulfoxide), ethanol, hydrogen peroxide (H_2O_2), HCl was purchased from Sigma-Aldrich, India and all the other chemicals were analytical grades and used without further purification.

2.2. Preparation of plant extract

Fresh leaves of *Acalypha Indica* were washed with running tap water and it was shade-dried. The leaves were powdered by using mechanical grinding. 20 g of coarse leaf powder was taken in 100 ml ethanol and stirred at room temperature. After incubation, it was filtered thoroughly using whatmann No.1 filter paper. The filtrate was used for the synthesis of copper oxide (Berra et al., 2018).

2.3. Preparation of Copper oxide (CuO) nanoparticles

10 ml of *Acalypha Indica* leaf extract was mixed with 90 ml of 0.1 M copper sulfate solution (Cu2+) dropwise with constant stirring at 60 °C for 2 h. The mixture color changed to brown precipitate, which indicates the formation of copper oxide nanoparticles. The solid product was washed with distilled water followed by ethanol to remove the impurities present in it and dried at 70 °C for 8 h. Finally, the dried powder was stored and used for further studies.

2.4. Preparation of Graphene oxide (GO)

Graphene oxide was synthesized from the oxygenation of graphite following the Hummers method (Abdolhosseinzadeh et al., 2015). The graphite flakes and $NaNO_3$ were taken in a 1:1 ratio which was then mixed in 50 ml H_2SO_4 (98%) in a round bottom flask and was kept under the ice bath with continuous stirring. After 120 min, potassium permanganate (6 g) was added slowly to the mixture at a temperature below 15 °C. Then the mixture was removed and stirred at a temperature of 35 °C for 24 h. After dilution, the temperature was rapidly increased to 98 °C till a brown colored solution appeared. The mixture was washed with 10% HCl and centrifuged, washed and filtered. The product was dried in a hot air oven to obtain graphene oxide powder.

2.5. Preparation of Graphene oxide – Copper oxide nanocomposites

Yellowish dispersion was obtained by dispersing 0.5 g of graphene oxide in the required quantity of distilled water. Later 0.2 g of Copper oxide nanoparticles were dispersed in the required quantity of distilled water and introduced into a yellowish-brown dispersion. Then the solution was stirred for about 4 h and centrifuged at 6000 rpm. The product was separated and then washed with ethanol and then placed in an oven for 8 h at 60 °C to yield the dried nanocomposite product.

2.6. Characterization of GO-CuO nanocomposites

The surface morphology of GO, CuO, GO-CuO nanocomposites was observed using FEI Quanta FEG200 (FESEM). Hi-resolution transmission electron microscope (JEOL Japan, JEM-2100 plus) at an operating voltage of 200 kV. Fourier transforms infrared (FTIR) analysis was performed in ALPHA-T-FT-IR Spectrometer. X-ray diffraction (XRD) measurements were carried out on a PAN analytical X-pert powder diffractometer using Cu-Kα radiation (λ = 0.15405 Å). X-ray photoelectron spectroscopy (XPS) was performed using a PHI versa probe III to characterize the surface chemical composition.

2.7. Anti-cancer activity of GO-CuO nanocomposites

We performed dimethyl thiazolyl tetrazolium bromide (MTT) assays to determine the quality of synthesized GO-CuO Nanocomposites and Copper oxide nanoparticles, cytotoxic to HCT116 cells. Approximately 1×10^4 cells were added to each well of the 96 well culture plate 95% air and 5% CO_2 in a humid atmosphere at 37° C for 24 h. HCT116 cells were treated with 25–100 µg/ml green synthesized Copper oxide nanoparticles and incubated for 36 h. Control cultures were treated with DMSO. After incubation time, 20 µl of MTT solution was added to each well and incubated for a further 4 h. Then 200 µl DMSO was added, and the absorption of the formed crystals was measured at 575 nm using an ELISA reader.

2.8. Photocatalytic activity

The photocatalytic activities of the CuO and GO–CuO nanocomposites were examined by the degradation of Methylene blue (MB) under visible irradiation. In this experiment, 20 mg of CuO catalysts were added into 50 ml of 20 mg/L of MB solution in a reaction vessel, which was stirred for about 30 min in the dark to achieve the absorption-desorption equilibrium. Then, the solution was exposed to the visible light irradiation using a 400 W Xenon lamp. The above same procedure was followed for synthesized nanocomposites. At a regular time interval, 2 ml of the reaction solution was sampled and analyzed by a UV–visible spectrophotometer (UV 2100, Shimadzu).

3. Results and discussion

3.1. Characterization of synthesized CuO-GO nanocomposites

The surface morphology of CuO-GO nanocomposites was studied by field emission scanning electron microscopy (FESEM) and EDX. Fig. 1 shows the FE-SEM images of the pure CuO and CuO-GO nanocomposites respectively. Fig. 1(a) shows that the SEM images of the synthesized Copper oxide nanoparticles. Data exposed that the studied samples were clustered with a rough surface. Also, observed, the images indicated that the NPs were both agglomerated and monodispersed with almost spherical morphologies. Such variation in particle shape and size distribution is associated with the chemical composition of the *Acalypha Indica* extract (Sebeia et al., 2019). EDX confirmed the presence of Oxygen and Copper in the powders. The presence of S and C observed in the powder could be ascribed to the carbon film used to support the CuO samples as well as residual contributions from the $CuSO_4$ precursor and leaf-based organic compounds that emanated from the aqueous extract (Sone et al., 2020). Fig. 1(b) shows that the crumpled and layered flakes were seen on the surface. Hence, the occurrence of flakes denotes that the graphene layers were completely oxidized to GO (Dubey et al., 2015). The GO sheets showed a distinctive crumpled morphology and paper-like structure with a single or a few layers. Fig. 1(c) show that the CuO NPs were randomly distributed on the GO surfaces with aggregation. GO is a layered material bearing oxygen-containing functional groups on their basal planes and edges (Szabó et al., 2006). These functional groups can act as anchor sites, and consequently, make NPs formed in situ attach on the surfaces and edges of GO sheets. The positive Cu2+ ions easily adsorb onto these negative GO sheets via the electrostatic force. However, as seen in Fig. 1(b–c) the EDX spectra confirm the existence of elements such as Cu, O, and C without any impurities. HR-TEM was further employed to conform to the morphology and structure of the samples. It can be seen clearly from Fig. 2(a–b) that the prepared nanoparticles are distributed on the GO sheet. The Transmission Electron Microscope (TEM) analysis for the

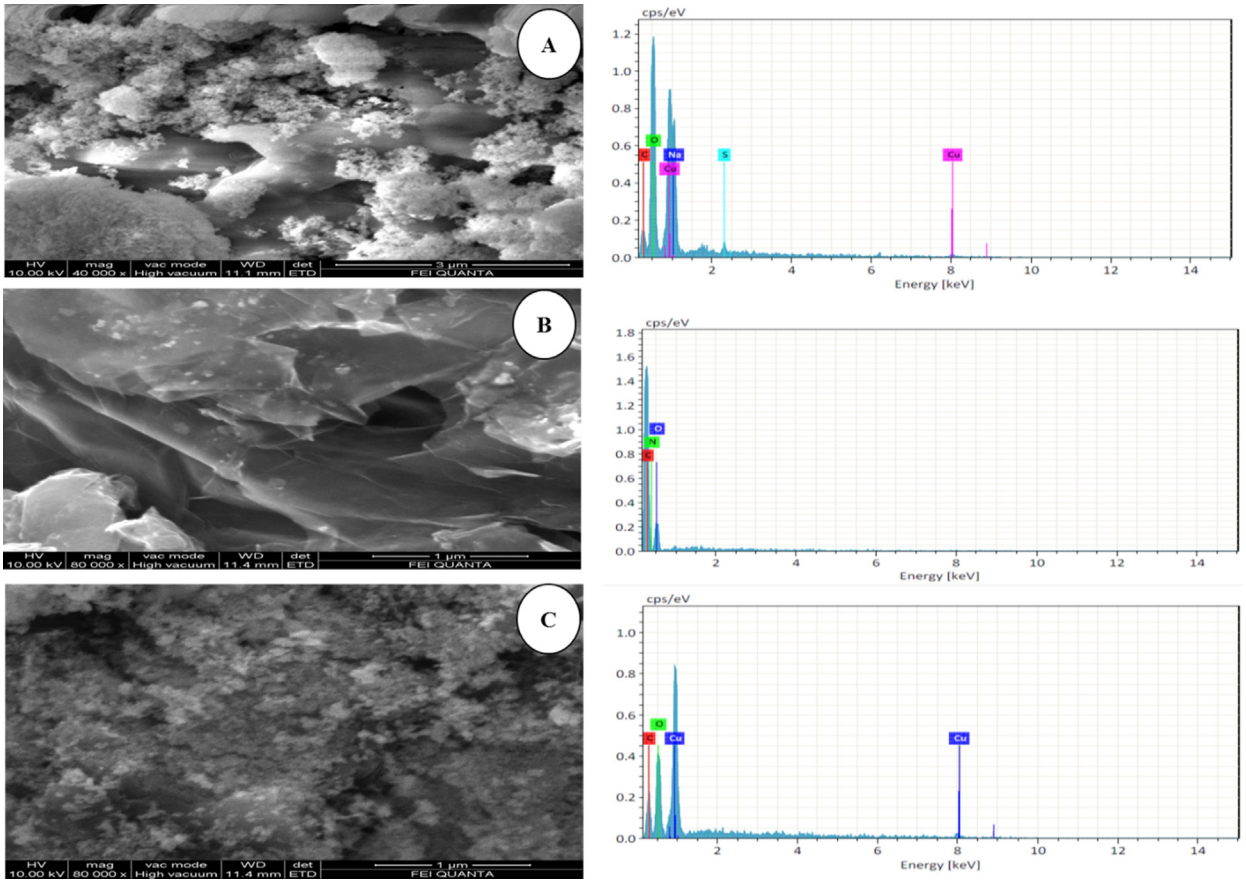

Fig. 1 SEM Images (A), CuO (B), GO and (C), GO-CuO Nanocomposites.

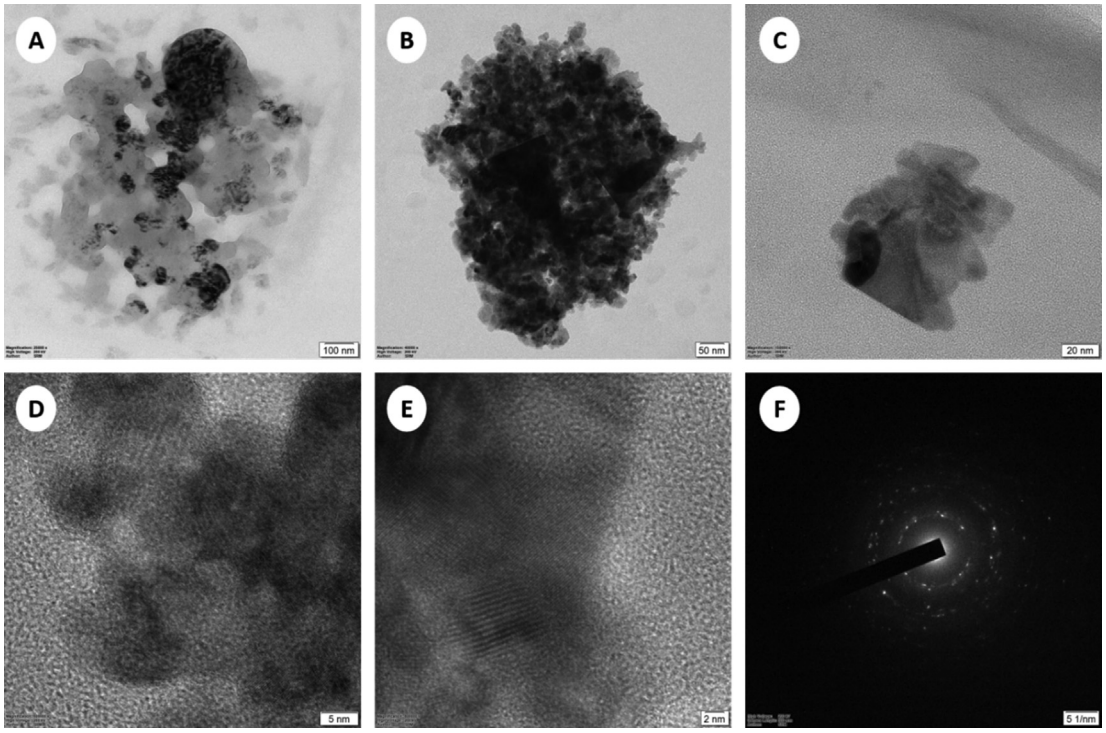

Fig. 2 TEM image of GO-CuO nanocomposites (A), 100 nm, (B), 50 nm, (C), 20 nm, (D), 5 nm, (E), 2 nm, and (F) SAED.

synthesized nanoparticles reports the crystalline nature of CuO NPs in agglomerated cluster structure as depicted in Fig. 2(c–e). The crystalline nature of the synthesized CuO NPs was confirmed by the selected area electron diffraction (SAED) indicated the formation of intermittent dots on the concentric circles in the SAED pattern as shown in the Fig. 2(f) this is very similar to those described in the previous reports (Nasrollahzadeh et al., 2015).

The FTIR spectra were used to investigate the structural nature and chemical composition of CuO and CuO-GO nanocomposites shown in (Fig. 3). The broad absorption peak at around 3362 cm^{-1} was due to the OH-stretching region (Kloprogge et al., 2004). The other peaks 1675 cm^{-1}, 1030 cm^{-1}, 1404 cm^{-1} corresponds to carbonyl stretching, O—H stretching, CH_2 asymmetric bending, and M—O—M bending (M═Cu) (Das et al., 2011). The characteristic peak of the IR spectra of CuO in the range of 400–600 cm^{-1} (Dehno Khalaji et al., 2012; Suramwar et al., 2012). The peaks at 526 cm^{-1} in the FTIR spectra reported for CuO-NPs which closely matches with our results (Padil and Černík, 2013). Consequently, the metal-oxygen frequencies observed for CuO-NPs are in close agreement with that of literature values. GO appears at the vibration and deformation bands of the OH group at 3372 cm^{-1}, a transmission band near 1616 cm^{-1}, assigned to physisorbed water (Szabó et al., 2006; Zhang et al., 2015) by hydrogen bonds. O—H bend appears in the region of 1375 cm^{-1}, the stretching vibration band of the C═O group at 1711 cm^{-1} (Kaniyoor et al., 2010). In the CuO-GO nanocomposites decrease in the intensity of the absorption peak (3423 cm^{-1}, 1593 cm^{-1}, 1418 cm^{-1}, 1248 cm^{-1}, and 1016 cm^{-1}) of GO implies the removal of the C═O (in carboxyl group) and O—H (hydroxyl group). In addition to that, the presence of Cu—O vibration mode around 503 cm^{-1} and 606 cm^{-1} represents the bond stretching, formation of bonds and vibrations between the nanocomposites as CuO NPs replaces the residual oxygen-containing functional group (Zhao et al., 2012).

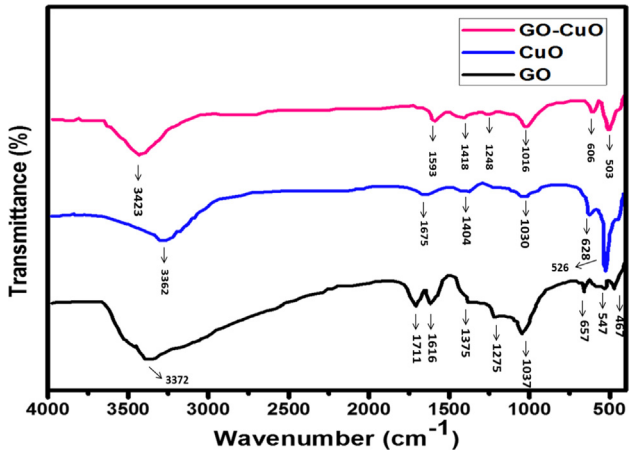

Fig. 3 FTIR spectra of GO, CuO, and GO-CuO Nanocomposites.

The optical properties of the combined CuO nanoparticles were investigated by UV–vis spectra in the wavelength range of 200–800 nm, as shown in (Fig. 4). while the absorption peak at 294 nm was related to CuO which confirmed the band gap was because of the intrinsic transition in CuO(Felix et al., 2015) it was found that graphene-oxide shows two absorption bands at 229 nm indicates π → π* transition of aromatic C—C bonds (Yang and Liu, 2011) and spectra at 295 nm indicates the n → π* transition (Dhara et al., 2015) CuO-GO

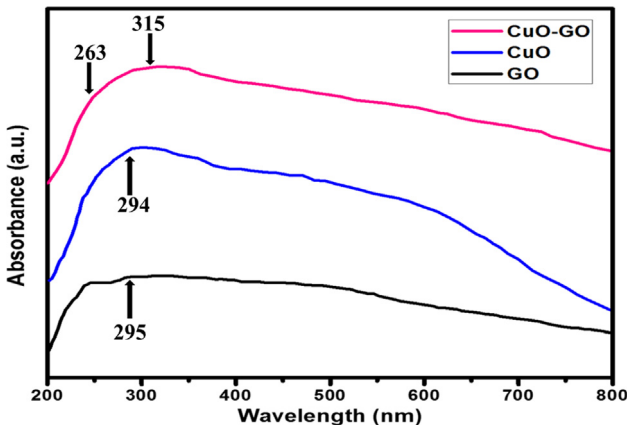

Fig. 4 UV–vis spectra of GO, CuO, and GO-CuO Nanocomposites.

nanocomposites showed a broad overlapping band from 263 to 315 nm which covers the band equivalent to GO and CuO nanoparticles. Henceforth, the absorption spectra show the formation of CuO and CuO-GO nanocomposites.

The XRD patterns of CuO and GO-CuO nanocomposite is shown in (Fig. 5). GO shows diffraction peaks at around 2θ = 12.66° and 42.82° corresponding to the (001) and (101) reflection plane. In which 2θ = 12.66° corresponding to the (001) reflection of GO, shows the interlayer spacing (0.84 nm) is higher than that of primeval graphite (about 0.34 nm) owed to the overview of oxygen-containing functional groups on the graphite sheet surfaces. Pure CuO exhibited diffraction peaks at 2θ = 32.44°, 35.42°, 38.69°, 48.80°, 53.36°, 58.20°, 61.47°, and 66.16° corresponds to the (110), (111), (200), (202), (020), (021), (113), and (311) crystal planes, respectively. They are related to the characteristic diffractions of the monoclinic phase of CuO (JCPDS 48-1548), wherever the (001) reflection peak of the layered GO almost disappeared. It was proposed that the diffraction peak would not be noticeable when GO was exfoliated. In this composite, the CuO

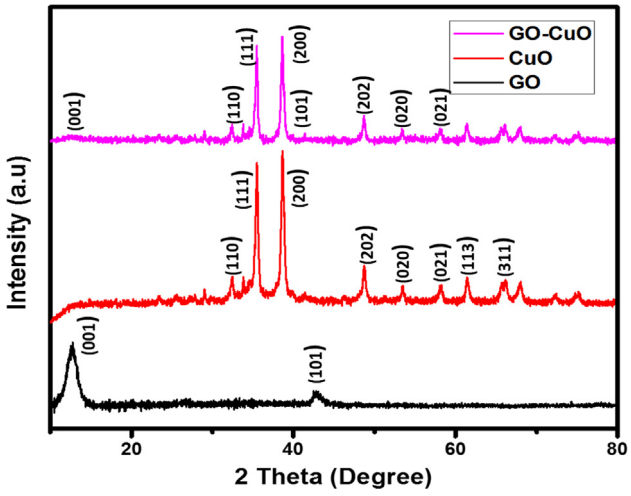

Fig. 5 XRD patterns of GO, CuO, and GO-CuO Nanocomposites.

dominated the GO layer, as shown by SEM studies (Zhu et al., 2010; Bradder et al., 2011) we investigated the XRD pattern of GO-CuO nanocomposites, the 2 θ = 36.0°, 52.1°, 43.28°, 16.22°, 65.05°, 62.02° and corresponds to (110), (111), (200), (101), (202), (020). Accordingly, the carbonyl groups of both carboxylic acids and ketones present on GO were powerfully coordinated with Cu metal ions that form a layer-on-layer network. The resulting GO-CuO nanocomposites had a porous 3D network that increased the hydrophilicity. No additional characteristic peaks of impurities were observed. The GO peaks are not visible in the CuO-GO nanocomposite, which may be due to the overlap with the 12.66 and 42.82 peaks of CuO and or a lower amount of highly dispersed GO in the composite.

The chemical states of the elements present in the GO-CuO nanocomposites were studied by X-ray photoelectron spectroscopy (XPS). The survey spectrum Fig. 6(a) displays the surface binding situation, carbon, oxygen, and copper elements in the nanocomposites. Fig. 6(b) shows the carbon peaks are deconvoluted into two peaks, where the primary C—C bond generated shown at 283.1 eV. The graphene oxide is further verified by the C—O bond at 286.3 eV (Deo et al., 2011). Copper has a binding energy of 934.8 eV (Cu $2p_{3/2}$) and 954.7 eV (Cu $2p_{1/2}$) respectively, these signals reveal the occurrence of Cu2+ chemical state in the CuO particles (Bao et al., 2011). The gap between the (Cu $2p_{3/2}$) and (Cu $2p_{1/2}$) level is about 20 eV that is in the bargain with the typical spectrum of CuO. Fig. 6(d) also shows one additional shake-up peaks at 943.29, signifying the occurrence of an unfilled Cu 3d shell and thus promote authorizing the existence of Cu2+ in the sample which is positioned at higher binding energies compared to those of the main peaks. The Oxygen 1s characteristic peaks of the sample shown in Fig. 6(c) the typical peaks of the copper-oxygen bond (O—Cu and Cu—O—Cu) at about 524.4 eV, 531.8 eV, respectively.

3.2. In-vitro studies on HCT-116 cells

The cytotoxicity of CuO and GO-CuO nanocomposites was performed by testing the viability of HCT-116 cells and it was shown in Fig. 7(a). In the present study, the synthesized CuO and GO-CuO nanocomposites were taken in various concentrations like 25, 50, 75, 100 μg/mL after incubation for 24 h. The percentage of cell viability was calculated from the OD value of MTT assay as shown in (Table 1). The prepared CuO and GO-CuO nanocomposites have shown poor cytotoxicity effect on the HCT-116 cell line at an initial concentration (25 μg/mL) shows 94.54% and 92.42% cell viability. Subsequently increasing the concentration of synthesized nanocomposites (CuO, and GO-CuO) the viability of cancer cells decreased. At higher concentration of nanoparticles and nanocomposites (100 μg/mL) exhibits 35.39% and 31.81% of cell viability respectively which proved that the synthesized nanocomposites have significant anticancer activity against HCT-116 cancer cell line. IC_{50} value for the CuO nanoparticle is 53.77 μg/mL where as the IC_{50} value for the CuO-GO nanocomposites is 46.31 μg/mL. One of the major benefits of combination therapies is probable for providing synergistic effects. In combination therapy the total therapeutic benefit of the drugs in combination were found to be greater than the sum of the effects of the drugs individually. These

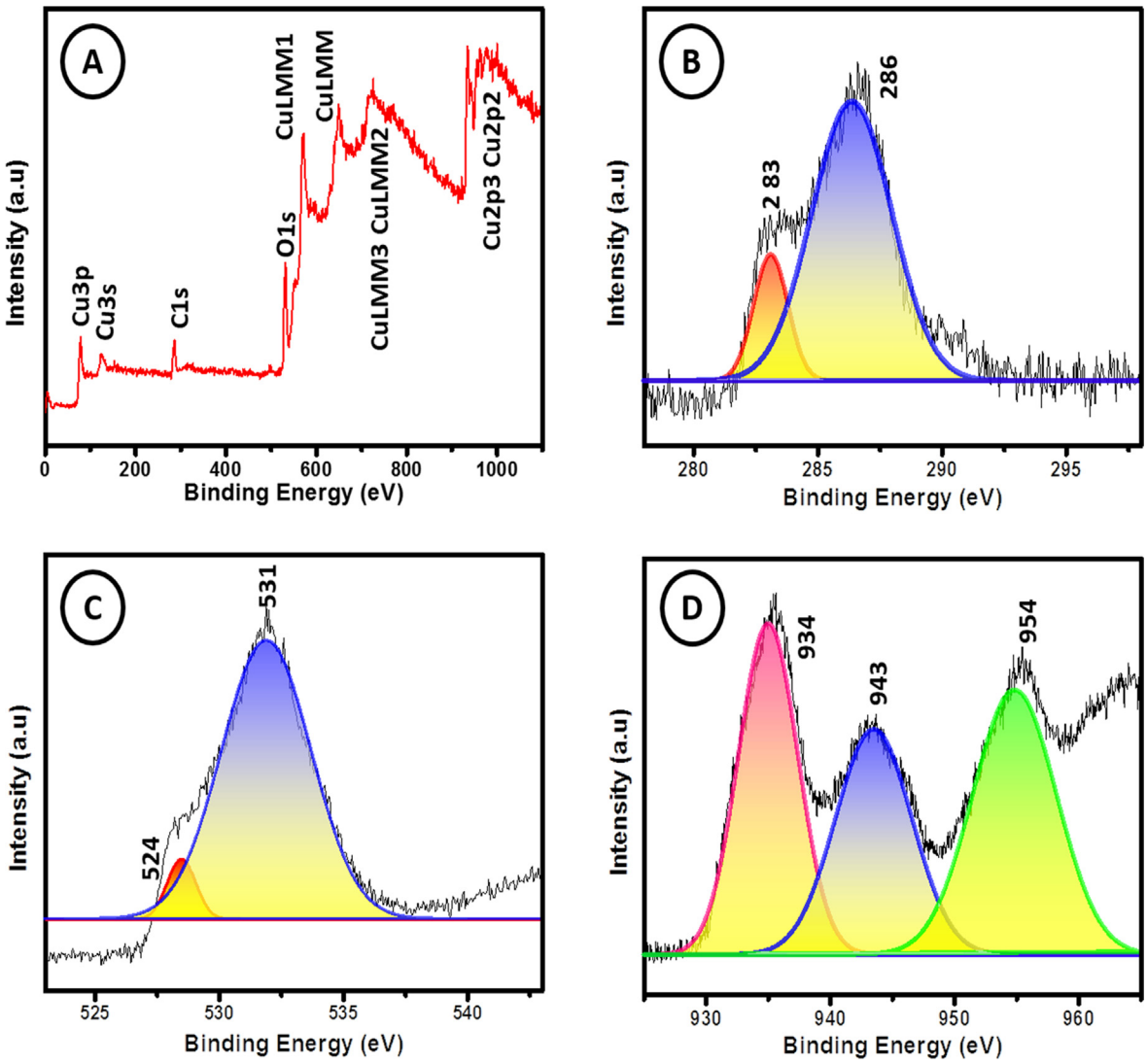

Fig. 6 XPS spectrum of GO-CuO nanocomposites.

recompenses have driven drug discovery efforts toward the search for combination therapies. The best drug combination with maximal antitumor efficacy can be calculated by combination index (CI) isobologram analysis/ multiple drug effect, an effective way to demonstrate that drugs are working synergistically (Chou, 2010). CuO NPs drug acts through a particular pathway, whereas CuO-GO nanocomposites drug can show enhanced anticancer activity by acting through several pathways. In the case of CuO NPs drug treatment, MDR proteins such as P-gp efflux drug out of the cell, whereas for CuO-GO nanocomposites formulations P-gp inhibitor blocks the role of MDR proteins and increases the intracellular concentration of other co-administered drugs resulting in higher efficacy by overcoming the MDR phenotype. High dose is needed for CuO NPs drug treatment and consequently results in toxicity to the normal cells, whereas treatment with CuO-GO nanocomposites drug combinations by synergistic action can reduce the dose of each single drug and thereby decrease the toxicity (Parhi et al., 2012). GO acted as the tumor inhibitor and drug delivery carrier (Cheng et al., 2015), respectively. The CuO-GO nanocomposites are considered carriers for phytocompounds and may act as anticancer agents. Cell membranes (Cancer / normal) carry negatively charged materials such as lipids while nanocomposites carry positive charges with opposite charges and are responsible for the uptake and internalization of nanocomposites. The nanocomposite surface area is the most important factor in cell internalization. The cytotoxic activity through the production of ROS through activation caspase cascade of apoptosis, DNA damage and mitochondrial dysfunction (He et al., 2016; Jeyaraj et al., 2013; Austin et al., 2011; Arora et al., 2008). The possible mechanisms of anticancer activity of CuO-GO nanocomposites are diagrammatically represented in Fig. 7(b).

3.3. Photocatalytic activity against methylene blue (MB) dye

When the light irradiates on the nanocomposites (GO-CuO) catalyst, the photogenerated electron-hole pairs get divided for both GO and CuO. The electrons present in the conduction band of copper oxide recombine with the holes of the valence band of graphene oxide and the electrons remain left in the conduction band of GO which effectively reacts with the

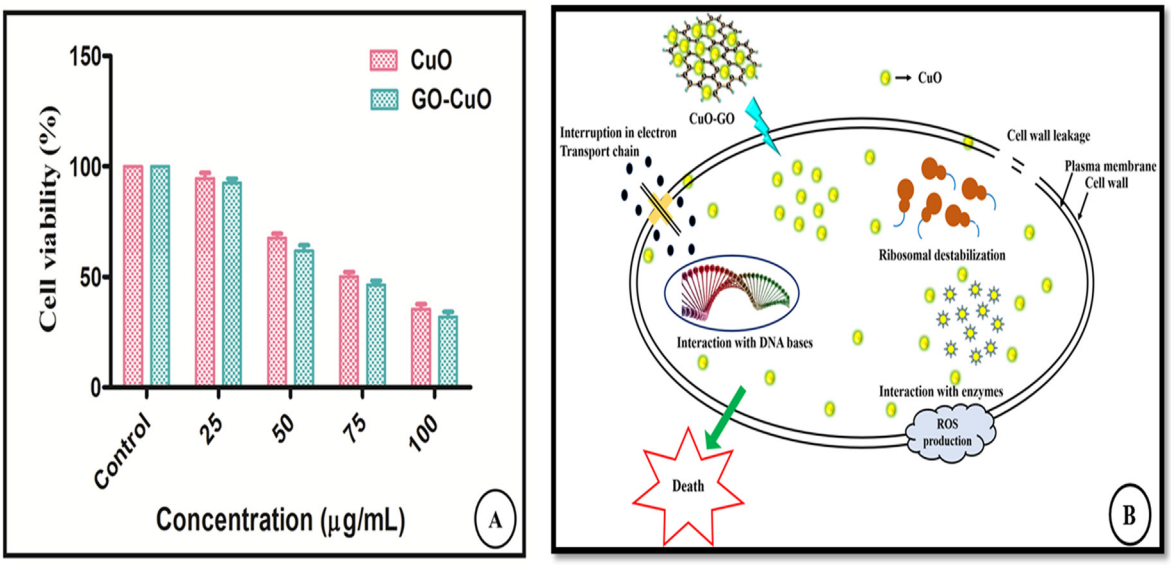

Fig. 7 *Invitro* cytotoxicity of CuO and GO-CuO nanocomposites was performed by testing the viability of HCT-116 cell line in different concentration 25 µg/mL, 50 µg/mL, 75 µg/mL, and 100 µg/mL for incubation of 24 h (A), The possible mechanism of anticancer activity of CuO-GO nanocomposites (B).

Table 1 Anticancer activity report of CuO and GO-CuO nanocomposites.

Concentration of CuO Nanoparticles (µg/mL)	Cell viability (%)	Concentration of GO-CuO Nanocomposites (µg/mL)	Cell viability (%)
0	100	0	100
25	94.54 ± 2.5	25	92.42 ± 2.0
50	67.57 ± 2.0	50	61.81 ± 2.4
75	50.18 ± 2.0	75	46.33 ± 2.0
100	35.39 ± 2.3	100	31.81 ± 2.3

oxygen to form reactive oxide radicals O_2^-. This then conventionally oxidizes the methylene blue dye. Also, $^{\cdot}O_2^-$ reacts with a water molecule to form hydroxyl radicals ($^{\cdot}OH$) (Tong et al., 2015). The photo generated holes (h +) in the valence band of CuO reacts with an H_2O molecule to produce $^{\cdot}OH$ radicals. The $^{\cdot}OH$ and $^{\cdot}O_2^-$ radicals are strong oxidative species that degrade methylene blue dye molecules. In the presence of CuO nanoparticles Fig. 8(a), 75% methylene blue (MB) dye was degraded. When CuO-GO nanocomposite, in methylene blue solution was exposed to visible light, the dye was decomposed 83.20% of MB in 60 min. It can be detected that the absorbance maxima of MB do not present a shift in the position with time evolution. In addition to adsorption capacity, the photocatalytic efficiency mainly depends upon the energy gained by electrons for photoexcitation and the lifetime of a photo-excited electron in the excited state. The photocatalytic activity of CuO nanoparticles might arise owing to their low band-gap energy, surface area and defect centers, created by oxygen vacancies (Gao et al., 2013; Chang et al., 2012, Bai et al., 2013). Though, CuO-GO nanocomposite shows impressive improvement in photodegradation of methylene blue and degrades the dye, almost completely. Fig. 8(b) shows that the solution is entirely degraded in 60 min. Fig. 8(c) shows the error bar diagram of CuO-GO nanocomposite. This excellent photocatalytic activity achieved by CuO-GO is likely due to the synergetic effects of CuO nanoparticles and GO. GO act as electron acceptor material and provide the transport network, and serve to delay the electron-hole recombination which is a crucial factor for improvement of the performance of the photocatalyst (Zhang et al., 2010). The presence of GO in nanocomposite form enhances the surface area as compared to only CuO. This factor stimulates the efficient adsorption of dye molecules on the surface of photocatalyst (Zhang et al., 2010). Therefore, the addition of an appropriate amount of GO is the major factor for the significant enhancement of photocatalytic activity (Hu and Tang, 2013). The possible photocatalytic degradation mechanism for MB dye solution over CuO-GO nanocomposites was explained as follows based on the aforementioned results as shown in Fig. 8(d). Once nanocomposites CuO-GO were irradiated with UV–Visible light, the electron excited from the valence band (VB) to CuO's conduction band (CB), leaving holes in the valence band behind. During the photocatalytic reaction, these photo-excited electrons may pass from the CB to the GO surface which suppresses the electron-hole recombination levels. Also, the photo-generated electrons and holes may react with water and oxygen molecules absorbed from the surface and produce the reactive species to degrade the dye molecules in the solution. During this time the photocatalytic chemical reactions were explained as follows

$$CuO/GO + hv \rightarrow CuO/GO\ (e^- + h^+) \quad (1)$$

$$GO + e^- \rightarrow GO\ (e^-) \quad (2)$$

$$O_2 + CuO\ (e-) \rightarrow O_2.^- \quad (3)$$

$$O_2 + GO\ (e-) \rightarrow O_2.^- \quad (4)$$

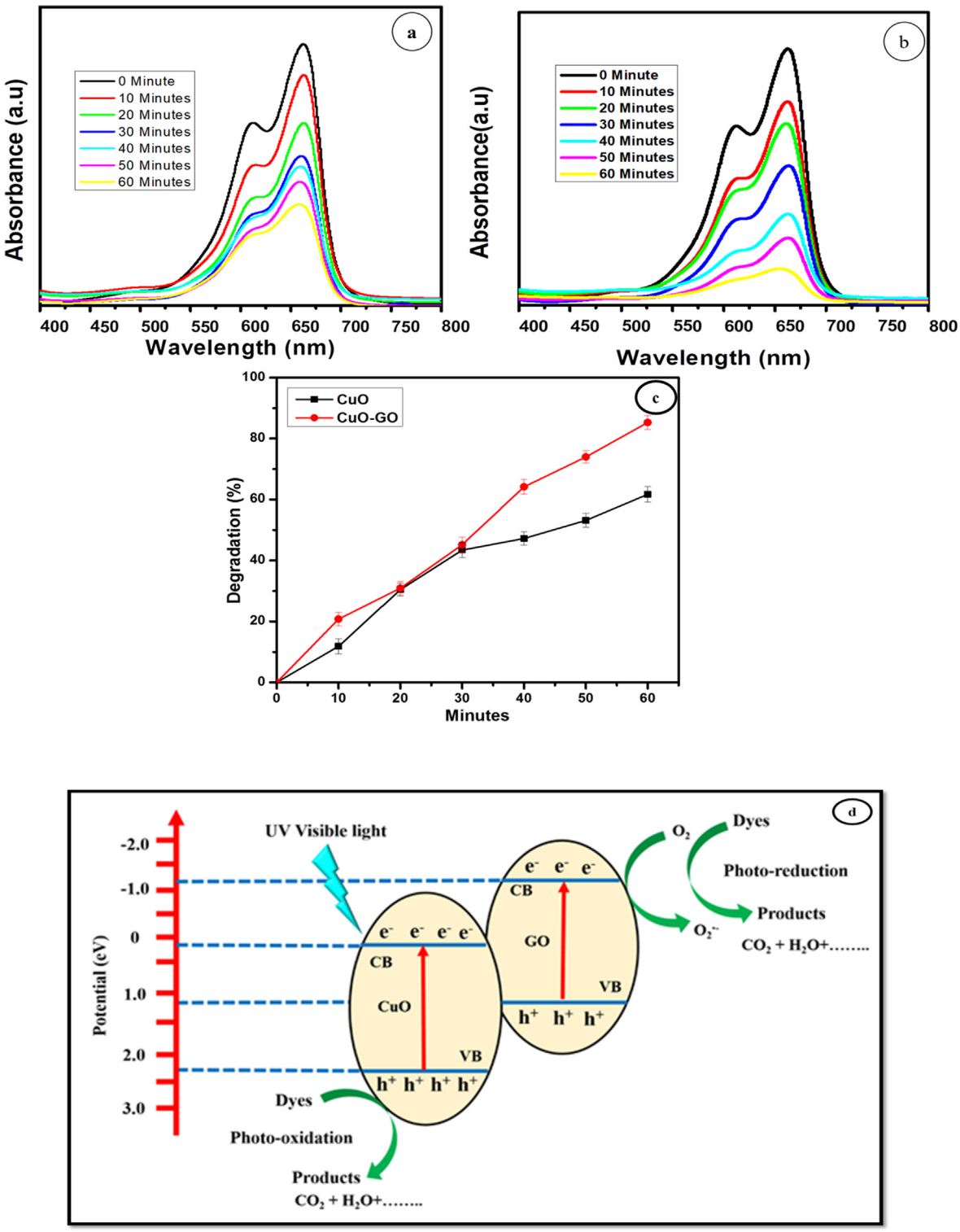

Fig. 8 Photo catalytic degradation of (a) CuO, (b) GO-CuO nanocomposites, (c) Percentage degradation of methylene blue with nanocomposites, (d) possible mechanism for dye degradation of MB.

$$CuO/GO\ (h^+) + (OH^-) \rightarrow CuO/GO + (OH^{\cdot}) \quad (5)$$

$$^{\cdot}OH + \text{pollutant (MB)} \rightarrow \text{Degradation product} \quad (6)$$

$$^{\cdot}O_2 + \text{pollutant (MB)} \rightarrow \text{Degradation product} \quad (7)$$

4. Conclusion

This work reports the fabrication of CuO nanoparticles and CuO-GO nanocomposites by the green method which consumes highly profuse, eco-friendly *Acalypha indica*. No periph-

eral capping/reducing agents are required in this synthesis. As the biomolecules present in *Acalypha Indica* leaf extract acted as reducing/capping agents thereby giving rise to CuO nanoparticles. All though, the formation of CuO-GO nanocomposite, the anchoring of CuO nanoparticles on GO nanosheets took place owing to the H-bonding between the functional group present in Graphene Oxide and electrostatic interactions, π → π interactions. The TEM, SEM shows that the CuO- GO nanocomposites were randomly anchored onto the graphene sheets. while the absorption peak at 294 nm was related to CuO which confirmed the band gap was because of the intrinsic transition in CuO. It was found that graphene-oxide shows two absorption bands at 229 nm. The peaks at 526 cm^{-1} in the FTIR spectra reported for CuO-NPs. GO appears at the vibration and deformation bands of the OH group at 3372 cm-1. In XRD GO shows diffraction peaks at around 2θ = 12.66° and 42.82° corresponding to the (001) and (101) reflection plane. CuO exhibits diffraction peaks at 2θ = 32.44°, 35.42°, 38.69°, 48.80°, 53.36°, 58.20°, 61.47°, and 66.16° corresponds to the (110), (111), (200), (202), (020), (021), (113), and (311) crystal planes, The graphene oxide is further verified by the C-O bond at 286.3 eV. Copper has binding energy of 934.8 eV (Cu $2p_{3/2}$) and 954.7 eV (Cu $2p_{1/2}$). Also, this article proved the prospective of CuO nanoparticle and CuO-GO nanoComposite as a catalyst in photocatalytic activity and anti-cancer activity. cytotoxic activity was found to be 70% against HCT-116 Human colon cancer cell lines at 100 μg/ml. The photocatalytic studies revealed that synthesized nanocomposites have the efficiency to degrade methylene blue dye by 83.20%. In all the applications, CuO-GO Nanocomposite exhibited higher efficiency paralleled to CuO NPs owed to the presence of GO sheets which makes the electron transfer processes much faster thereby enhancing the rate of reactions oddly. It is owing to a small bandgap with a wide surface area of CuO-GO nanocomposite and inhibition of electron-hole recombination. CuO- GO as cost-efficient, easy to prepare, effective photocatalyst and it might be valid at industrial scale for the photocatalysis of other industrial dyes and biological applications.

Declaration of Competing Interest

The authors declare that they have no known competing financial interests or personal relationships that could have appeared to influence the work reported in this paper.

Acknowledgment

The authors wish to acknowledge DST-FIST (fund for improvement of S&T) for the financial assistance at the Department of Chemistry, SRM Institute of Science and Technology (grant no SR/FST/CST-266/2015(c))

References

Abdolhosseinzadeh, S., Asgharzadeh, H., Kim, H.S., 2015. Fast and fully-scalable synthesis of reduced graphene oxide. Sci. Rep. 5, 10160.

Abiraman, T., Ramanathan, E., Kavitha, G., Rengasamy, R., Balasubramanian, S., 2017. Synthesis of chitosan capped copper oxide nanoleaves using high intensity (30 kHz) ultrasound sonication and their application in antifouling coatings. Ultrason. Sonochem. 34, 781–791.

Alade, P.I., Irobi, O.N., 1993. Antimicrobial activities of crude leaf extracts of Acalypha wilkesiana. J. Ethnopharmacol. 39, 171–174.

Alizadeh, T., Mirzagholipur, S., 2014. A Nafion-free non-enzymatic amperometric glucose sensor based on copper oxide nanoparticles–graphene nanocomposite. Sensors Actuators B Chem. 198, 438–447.

Almeida, N.A., Martins, P.M., Teixeira, S., da Silva, J.A.L., Sencadas, V., Kühn, K., Cuniberti, G., Lanceros-Mendez, S., Marques, P.A.A.P., 2016. TiO 2/graphene oxide immobilized in P (VDF-TrFE) electrospun membranes with enhanced visible-light-induced photocatalytic performance. J. Mater. Sci. 51, 6974–6986.

Annanouch, F.E., Haddi, Z., Vallejos, S., Umek, P., Guttmann, P., Bittencourt, C., Llobet, E., 2015. Aerosol-assisted CVD-grown WO3 nanoneedles decorated with copper oxide nanoparticles for the selective and humidity-resilient detection of H2S. ACS Appl. Mater. Interfaces 7, 6842–6851.

Arora, S., Jain, J., Rajwade, J.M., Paknikar, K.M., 2008. Cellular responses induced by silver nanoparticles: in vitro studies. Toxicol. Lett. 179, 93–100.

Asfaram, A., Dil, E.A., Arabkhani, P., Sadeghfar, F., Ghaedi, M., 2020. Magnetic Cu: CuO-GO nanocomposite for efficient dispersive micro-solid phase extraction of polycyclic aromatic hydrocarbons from vegetable, fruit, and environmental water samples by liquid chromatographic determination. Talanta 121131.

Austin, L.A., Kang, B., Yen, C.-W., El-Sayed, M.A., 2011. Nuclear targeted silver nanospheres perturb the cancer cell cycle differently than those of nanogold. Bioconjug. Chem. 22, 2324–2331.

Bai, H., Su, N., Li, W., Zhang, X., Yan, Y., Li, P., Ouyang, S., Ye, J., Xi, G., 2013. W 18 O 49 nanowire networks for catalyzed dehydration of isopropyl alcohol to propylene under visible light. J. Mater. Chem. A 1, 6125–6129.

Bansal, V., Bharde, A., Ramanathan, R., Bhargava, S.K., 2012. Inorganic materials using 'unusual'microorganisms. Adv. Colloid Interface Sci. 179, 150–168.

Bao, L., Zhang, Z.L., Tian, Z.Q., Zhang, L., Liu, C., Lin, Y., Qi, B., Pang, D.W., 2011. Electrochemical tuning of luminescent carbon nanodots: From preparation to luminescence mechanism. Adv. Mater. 23, 5801–5806.

Berra, D., Laouini, S.E., Benhaoua, B., Ouahrani, M.R., Berrani, D., Rahal, A., 2018. Green synthesis of copper oxide nanoparticles by pheonix dactylifera L leaves extract. Dig. J. Nanomater. Biostruct. 13, 1231–1238.

Bhattacharjee, A., Morya, V., Ghoroi, C., 2020. Enzyme-mimetic activity of sugar cane juice stabilized CuO nanospheres and CuO/GO nanocomposite: green synthesis and applications. Colloid Interface Sci. Commun. 35, 100239.

Bordbar, M., Sharifi-Zarchi, Z., Khodadadi, B., 2017. Green synthesis of copper oxide nanoparticles/clinoptilolite using Rheum palmatum L. root extract: high catalytic activity for reduction of 4-nitro phenol, rhodamine B, and methylene blue. J. Sol-Gel Sci. Technol. 81, 724–733.

Bradder, P., Ling, S.K., Wang, S., Liu, S., 2011. Dye adsorption on layered graphite oxide. J. Chem. Eng. Data 56, 138–141.

Chandrasekaran, S., 2013. A novel single step synthesis, high efficiency and cost effective photovoltaic applications of oxidized copper nano particles. Sol. Energy Mater. Sol. Cells 109, 220–226.

Chang, X., Sun, S., Dong, L., Yin, Y., 2012. Efficient synthesis of Ag/AgCl/W18O49 nanorods and their antibacterial activities. Mater. Lett. 83, 133–135.

Chaudhary, S., Rohilla, D., Umar, A., Kaur, N., Shanavas, A., 2019. Synthesis and characterizations of luminescent copper oxide nanoparticles: toxicological profiling and sensing applications. Ceram. Int. 45, 15025–15035.

Cheng, R., Zou, R., Ou, S., Guo, R., Yan, R., Shi, H., Yu, S., Li, X., Bu, Y., Lin, M., 2015. Graphene oxide complex as a pH-sensitive antitumor drug. Polym. Chem. 6, 2401–2406.

Chengaiah, B., Kumar, K.M., Alagusundaram, M., Sasikala, C., Chetty, C.M., 2009. In vitro anthelmintic activity of roots of Acalypha indica Linn. Int. J. pharmtech Res. 1, 1499–1502.
Chou, T.-C., 2010. Drug combination studies and their synergy quantification using the Chou-Talalay method. Cancer Res. 70, 440–446.
Das, A.K., Ahmed, F., Biswas, N.N., Dev, S., Masud, M.M., 2005. Diuretic activity of Acalypha indica. Dhaka Univ. J. Pharm. Sci., 4
Das, R., Nath, S.S., Bhattacharjee, R., 2011. Synthesis of linoleic acid capped copper nanoparticles and their fluorescence study. J. Fluoresc. 21, 1165–1170.
Das, S.K., Chandra, B.K., Molla, R.A., Sengupta, M., Islam, S.M., Majee, A., Bhaumik, A., 2020. CuO grafted triazine functionalized covalent organic framework as an efficient catalyst for CC homo coupling reaction. Mol. Catal. 480, 110650.
Dehno Khalaji, A., Jafari, K., Maghsodlou Rad, S., 2012. Solid-state thermal decoposition method for the preparation of CuO nanoparticles. J. Nanostruct. 2, 505–508.
Deo, M., Mujawar, S., Game, O., Yengantiwar, A., Banpurkar, A., Kulkarni, S., Jog, J., Ogale, S., 2011. Strong photo-response in a flip-chip nanowire p-Cu 2 O/n-ZnO junction. Nanoscale 3, 4706–4712.
Dhara, K., Ramachandran, T., Nair, B.G., Babu, T.G.S., 2015. Single step synthesis of Au–CuO nanoparticles decorated reduced graphene oxide for high performance disposable nonenzymatic glucose sensor. J. Electroanal. Chem. 743, 1–9.
Dubey, S.P., Nguyen, T.T.M., Kwon, Y.-N., Lee, C., 2015. Synthesis and characterization of metal-doped reduced graphene oxide composites, and their application in removal of Escherichia coli, arsenic and 4-nitrophenol. J. Ind. Eng. Chem. 29, 282–288.
Felix, S., Chakkravarthy, R.B.P., Grace, A.N., 2015. Microwave assisted synthesis of copper oxide and its application in electrochemical sensing. In: IOP Conference Series: Materials Science and Engineering. IOP Publishing, p. 12115.
Gao, X., Xiao, F., Yang, C., Wang, J., Su, X., 2013. Hydrothermal fabrication of W 18 O 49 nanowire networks with superior performance for water treatment. J. Mater. Chem. A 1, 5831–5834.
Giri, S.D., Sarkar, A., 2016. Electrochemical study of bulk and monolayer copper in alkaline solution. J. Electrochem. Soc. 163, H252–H259.
He, Y., Du, Z., Ma, S., Liu, Y., Li, D., Huang, H., Jiang, S., Cheng, S., Wu, W., Zhang, K., 2016. Effects of green-synthesized silver nanoparticles on lung cancer cells in vitro and grown as xenograft tumors in vivo. Int. J. Nanomed. 11, 1879.
Hekmati, M., 2019. Application of biosynthesized CuO nanoparticles using Rosa canina fruit extract as a recyclable and heterogeneous nanocatalyst for alkyne/aldehyde/amine A 3 coupling reactions. Catal. Lett. 149, 2325–2331.
Hu, G., Tang, B., 2013. Photocatalytic mechanism of graphene/titanate nanotubes photocatalyst under visible-light irradiation. Mater. Chem. Phys. 138, 608–614.
Huang, Y., Chen, D., Hu, X., Qian, Y., Li, D., 2018. Preparation of TiO2/carbon nanotubes/reduced graphene oxide composites with enhanced photocatalytic activity for the degradation of rhodamine B. Nanomaterials 8, 1–9.
Ijaz, F., Shahid, S., Khan, S.A., Ahmad, W., Zaman, S., 2017. Green synthesis of copper oxide nanoparticles using Abutilon indicum leaf extract: antimicrobial, antioxidant and photocatalytic dye degradation activitie. Trop. J. Pharm. Res. 16, 743–753.
Ishak, F.D., So'ad, S.Z.M., Jauhari, A.H.A., Mashud, N.N., Hassan, N.M., 2013. In vitro study of antimicrobial activity of Acalypha Indica Linn. extract. Open Conf. Proc. J.
Jadhav, M.S., Kulkarni, S., Raikar, P., Barretto, D.A., Vootla, S.K., Raikar, U.S., 2018. Green biosynthesis of CuO & Ag–CuO nanoparticles from Malus domestica leaf extract and evaluation of antibacterial, antioxidant and DNA cleavage activities. New J. Chem. 42, 204–213.
Jeyaraj, M., Rajesh, M., Arun, R., MubarakAli, D., Sathishkumar, G., Sivanandhan, G., Dev, G.K., Manickavasagam, M., Premkumar, K., Thajuddin, N., 2013. An investigation on the cytotoxicity and caspase-mediated apoptotic effect of biologically synthesized silver nanoparticles using Podophyllum hexandrum on human cervical carcinoma cells. Colloids Surfaces B Biointerfaces 102, 708–717.
Jiang, G., Lin, Z., Chen, C., Zhu, L., Chang, Q., Wang, N., Wei, W., Tang, H., 2011. TiO2 nanoparticles assembled on graphene oxide nanosheets with high photocatalytic activity for removal of pollutants. Carbon N. Y. 49, 2693–2701. https://doi.org/10.1016/j.carbon.2011.02.059.
Jiang, W., Liu, Y., Wang, J., Zhang, M., Luo, W., Zhu, Y., 2016. Separation-free polyaniline/TiO2 3D hydrogel with high photocatalytic activity. Adv. Mater. Interfaces 3, 1500502.
Kaniyoor, A., Baby, T.T., Ramaprabhu, S., 2010. Graphene synthesis via hydrogen induced low temperature exfoliation of graphite oxide. J. Mater. Chem. 20, 8467–8469.
Kannan, S.K., Sundrarajan, M., 2015. Biosynthesis of Yttrium oxide nanoparticles using Acalypha indica leaf extract. Bull. Mater. Sci. 38, 945–950.
Kavitha, K.S., Baker, S., Rakshith, D., Kavitha, H.U., Yashwantha Rao, H.C., Harini, B.P., Satish, S., 2013. Plants as green source towards synthesis of nanoparticles. Int. Res. J. Biol. Sci. 2, 66–76.
Kerour, A., Boudjadar, S., Bourzami, R., Allouche, B., 2018. Eco-friendly synthesis of cuprous oxide (Cu2O) nanoparticles and improvement of their solar photocatalytic activities. J. Solid State Chem. 263, 79–83.
Khan, R., Ahmad, R., Rai, P., Jang, L.-W., Yun, J.-H., Yu, Y.-T., Hahn, Y.-B., Lee, I.-H., 2014. Glucose-assisted synthesis of Cu2O shuriken-like nanostructures and their application as nonenzymatic glucose biosensors. Sens. Actuators B Chem. 203, 471–476.
Kloprogge, J.T., Hickey, L., Frost, R.L., 2004. FT-Raman and FT-IR spectroscopic study of synthetic Mg/Zn/Al-hydrotalcites. J. Raman Spectrosc. 35, 967–974.
Li, C., Mou, S., Zhu, X., Wang, F., Wang, Y., Qiao, Y., Shi, X., Luo, Y., Zheng, B., Li, Q., 2019. Dendritic Cu: a high-efficiency electrocatalyst for N 2 fixation to NH 3 under ambient conditions. Chem. Commun. 55, 14474–14477.
Li, C.W., Ciston, J., Kanan, M.W., 2014. Electroreduction of carbon monoxide to liquid fuel on oxide-derived nanocrystalline copper. Nature 508, 504–507.
Liang, P., Wang, F., Hu, Z.-A., 2018. Controlled synthesis of ordered sandwich CuCo2O4/reduced graphene oxide composites via layer-by-layer heteroassembly for high-performance supercapacitors. Chem. Eng. J. 350, 627–636.
Manjari, G., Saran, S., Arun, T., Rao, A.V.B., Devipriya, S.P., 2017. Catalytic and recyclability properties of phytogenic copper oxide nanoparticles derived from Aglaia elaeagnoidea flower extract. J. Saudi Chem. Soc. 21, 610–618.
Martins, P.M., Gomez, V., Lopes, A.C., Tavares, C.J., Botelho, G., Irusta, S., Lanceros-Mendez, S., 2014. Improving photocatalytic performance and recyclability by development of Er-doped and Er/Pr-codoped TiO2/poly(vinylidene difluoride)–trifluoroethylene composite membranes. J. Phys. Chem. C 118, 27944–27953.
Maruthupandy, M., Zuo, Y., Chen, J.-S., Song, J.-M., Niu, H.-L., Mao, C.-J., Zhang, S.-Y., Shen, Y.-H., 2017. Synthesis of metal oxide nanoparticles (CuO and ZnO NPs) via biological template and their optical sensor applications. Appl. Surf. Sci. 397, 167–174.
Murugan, T., Saranraj, P., 2011. Antibacterial activity of various solvent extracts of the Indian herbal plant Acalypha indica against human pathogens causing nosocomial infection. Int. J. Pharm. Biol. Arch. 2, 1498–1503.
Nasrollahzadeh, M., Sajadi, S.M., Rostami-Vartooni, A., Hussin, S. M., 2016. Green synthesis of CuO nanoparticles using aqueous extract of Thymus vulgaris L. leaves and their catalytic performance for N-arylation of indoles and amines. J. Colloid Interface Sci. 466, 113–119.

Nasrollahzadeh, M., Sajadi, S.M., Rostami-Vartooni, A., Khalaj, M., 2015. Green synthesis of Pd/Fe3O4 nanoparticles using Euphorbia condylocarpa M. bieb root extract and their catalytic applications as magnetically recoverable and stable recyclable catalysts for the phosphine-free Sonogashira and Suzuki coupling reactions. J. Mol. Catal. A: Chem. 396, 31–39.

Nguyen, T.-T., Hwang, S.-Y., Vuong, N.M., Pham, Q.-T., Nghia, N. N., Kirtland, A., Lee, Y.-I., 2018. Preparing cuprous oxide nanomaterials by electrochemical method for non-enzymatic glucose biosensor. Nanotechnology 29, 205501.

Ochoa, L., Medina-Velo, I.A., Barrios, A.C., Bonilla-Bird, N.J., Hernandez-Viezcas, J.A., Peralta-Videa, J.R., Gardea-Torresdey, J. L., 2017. Modulation of CuO nanoparticles toxicity to green pea (Pisum sativum Fabaceae) by the phytohormone indole-3-acetic acid. Sci. Total Environ. 598, 513–524.

Padil, V.V.T., Černík, M., 2013. Green synthesis of copper oxide nanoparticles using gum karaya as a biotemplate and their antibacterial application. Int. J. Nanomed. 8, 889.

Parhi, P., Mohanty, C., Sahoo, S.K., 2012. Nanotechnology-based combinational drug delivery: an emerging approach for cancer therapy. Drug Discov. Today 17, 1044–1052.

Pendashteh, A., Mousavi, M.F., Rahmanifar, M.S., 2013. Fabrication of anchored copper oxide nanoparticles on graphene oxide nanosheets via an electrostatic coprecipitation and its application as supercapacitor. Electrochim. Acta 88, 347–357.

Praburaman, L., Jang, J.-S., Muthusamy, G., Arumugam, S., Manoharan, K., Cho, K.-M., Min, C., Kamala-Kannan, S., Byung-Taek, O., 2016. Piper betle-mediated synthesis, characterization, antibacterial and rat splenocyte cytotoxic effects of copper oxide nanoparticles. Artif. Cells Nanomedi. Biotechnol. 44, 1400–1405.

Prasad, K.S., Patra, A., Shruthi, G., Chandan, S., 2017. Aqueous extract of Saraca indica leaves in the synthesis of copper oxide nanoparticles: finding a way towards going green. J. Nanotechnol. 2017.

Prasad, K.P.S., Dhawale, D.S., Joseph, S., Anand, C., Wahab, M.A., Mano, A., Sathish, C.I., Balasubramanian, V.V., Sivakumar, T., Vinu, A., 2013. Post-synthetic functionalization of mesoporous carbon electrodes with copper oxide nanoparticles for supercapacitor application. Microporous Mesoporous Mater. 172, 77–86.

Prasad, P., Estari, M., 2014. Phytochemical and chromatographic studies in the leaves extract of Acalypha indica. Online Int. Interdiscip. Res. J. 4, 175–182.

Rahimi-Nasrabadi, M., Pourmortazavi, S.M., Davoudi-Dehaghani, A.A., Hajimirsadeghi, S.S., Zahedi, M.M., 2013. Synthesis and characterization of copper oxalate and copper oxide nanoparticles by statistically optimized controlled precipitation and calcination of precursor. CrystEngComm 15, 4077–4086.

Rajaselvam, J., Benila, S.J.M., Meena, R., 2012. A study of antimicrobial activity of Acalypha indica against selected microbial species. Int. J. Pharma Sci. Res. 3, 473–476.

Ramesh, P., Rajendran, A., Meenakshisundaram, M., 2014. Green syntheis of zinc oxide nanoparticles using flower extract cassia auriculata. J. Nanosci. Nanotechnol. 2, 41–45.

Reddy, T.R., Rao, R.S., Swamy, A.V., Reddanna, P., Reddy, G.P., Reddy, D.V., 2012. Exploring the anti-inflammatory and anticancer compounds from the leaves of Acalyphaindica. IOSR J. Pharm. Biol. Sci. 4, 1–7.

Sajan, C.P., Wageh, S., Al-Ghamdi, A.A., Yu, J., Cao, S., 2016. TiO2 nanosheets with exposed 001 facets for photocatalytic applications. Nano Res. 9, 3–27.

Sankar, R., Karthik, A., Prabu, A., Karthik, S., Shivashangari, K.S., Ravikumar, V., 2013. Origanum vulgare mediated biosynthesis of silver nanoparticles for its antibacterial and anticancer activity. Colloids Surfaces B Biointerfaces 108, 80–84.

Sankar, R., Manikandan, P., Malarvizhi, V., Fathima, T., Shivashangari, K.S., Ravikumar, V., 2014. Green synthesis of colloidal copper oxide nanoparticles using Carica papaya and its application in photocatalytic dye degradation. Spectrochim. Acta Part A Mol. Biomol. Spectrosc. 121, 746–750.

Sanseera, D., Niwatananun, W., Liawruangrath, B., Liawruangrath, S., Baramee, A., Trisuwan, K., Pyne, S.G., 2012. Antioxidant and anticancer activities from aerial parts of Acalypha indica Linn.

Sebeia, N., Jabli, M., Ghanmi, H., Ghith, A., Saleh, T.A., 2019. Effective dyeing of cotton fibers using Cynomorium Coccineum L. peel extracts: study of the influential factors using surface response methodology. J. Nat. Fibers, 1–13.

Sehar, S., Sher, F., Zhang, S., Khalid, U., Sulejmanović, J., Lima, E. C., 2020. Thermodynamic and kinetic study of synthesised graphene oxide-CuO nanocomposites: a way forward to fuel additive and photocatalytic potentials. J. Mol. Liq., 113494

Shabnam, L., Faisal, S.N., Roy, A.K., Haque, E., Minett, A.I., Gomes, V.G., 2017. Doped graphene/Cu nanocomposite: a high sensitivity non-enzymatic glucose sensor for food. Food Chem. 221, 751–759.

Shivkar, Y.M., Kumar, V.L., 2003. Anthelmintic activity of latex of Calotropis procera. Pharm. Biol. 41, 263–265.

Sivaraj, R., Rahman, P.K.S.M., Rajiv, P., Salam, H.A., Venckatesh, R., 2014. Biogenic copper oxide nanoparticles synthesis using Tabernaemontana divaricate leaf extract and its antibacterial activity against urinary tract pathogen. Spectrochim. Acta Part A Mol. Biomol. Spectrosc. 133, 178–181.

Sone, B.T., Diallo, A., Fuku, X.G., Gurib-Fakim, A., Maaza, M., 2020. Biosynthesized CuO nano-platelets: physical properties & enhanced thermal conductivity nanofluidics. Arab. J. Chem. 13, 160–170.

Sulaiman, G.M., Mohammed, W.H., Marzoog, T.R., Al-Amiery, A. A.A., Kadhum, A.A.H., Mohamad, A.B., 2013. Green synthesis, antimicrobial and cytotoxic effects of silver nanoparticles using Eucalyptus chapmaniana leaves extract. Asian Pac. J. Trop. Biomed. 3, 58–63.

Suramwar, N.V., Thakare, S.R., Khaty, N.T., 2012. Synthesis and catalytic properties of nano CuO prepared by soft chemical method. Int. J. Nano Dimens. 3, 75–80.

Szabó, T., Berkesi, O., Forgó, P., Josepovits, K., Sanakis, Y., Petridis, D., Dékány, I., 2006. Evolution of surface functional groups in a series of progressively oxidized graphite oxides. Chem. Mater. 18, 2740–2749.

Tkach, A., Matsukovich, A., Krekoten, N., Tabulina, L., Labunov, V., Radziuk, D., 2020. Graphene oxide-coated CuO nanoparticles for functionalization of acetylsalicylic acid and diclofenac. ACS Appl. Nano Mater.

Tong, Z., Yang, D., Shi, J., Nan, Y., Sun, Y., Jiang, Z., 2015. Three-dimensional porous aerogel constructed by g-C3N4 and graphene oxide nanosheets with excellent visible-light photocatalytic performance. ACS Appl. Mater. Interfaces 7, 25693–25701.

Vaidehi, D., Bhuvaneshwari, V., Bharathi, D., Sheetal, B.P., 2018. Antibacterial and photocatalytic activity of copper oxide nanoparticles synthesized using Solanum lycopersicum leaf extract. Mater. Res. Express 5, 85403.

Veisi, H., Hemmati, S., Javaheri, H., 2017. N-Arylation of indole and aniline by a green synthesized CuO nanoparticles mediated by Thymbra spicata leaves extract as a recyclable and heterogeneous nanocatalyst. Tetrahedron Lett. 58, 3155–3159.

Venkataprasanna, K.S., Prakash, J., Vignesh, S., Bharath, G., Venkatesan, M., Banat, F., Sahabudeen, S., Ramachandran, S., Venkatasubbu, G.D., 2020. Fabrication of Chitosan/PVA/GO/CuO patch for potential wound healing application. Int. J. Biol. Macromol. 143, 744–762.

Wang, T., Zhang, X., Zhu, X., Liu, Q., Lu, S., Asiri, A.M., Luo, Y., Sun, X., 2020. Hierarchical CuO@ ZnCo LDH heterostructured nanowire arrays toward enhanced water oxidation electrocatalysis. Nanoscale 12, 5359–5362.

Wang, Y., Yang, F., Zhang, H.X., Zi, X.Y., Pan, X.H., Chen, F., Luo, W.D., Li, J.X., Zhu, H.Y., Hu, Y.P., 2013. Cuprous oxide

nanoparticles inhibit the growth and metastasis of melanoma by targeting mitochondria. Cell Death Dis. 4. e783–e783.

Wei, W., Liu, D., Wei, Z., Zhu, Y., 2017. Short-range π-π stacking assembly on P25 TiO2 nanoparticles for enhanced visible-light photocatalysis. ACS Catal. 7, 652–663. https://doi.org/10.1021/acscatal.6b03064.

Wu, N., Zhang, C., Wang, C., Song, L., Yao, W., Gedanken, A., Lin, X., Shi, D., 2018. Zinc-doped copper oxide nanocomposites reverse temozolomide resistance in glioblastoma by inhibiting AKT and ERK1/2. Nanomedicine 13, 1303–1318.

Wu, T., Li, X., Zhu, X., Mou, S., Luo, Y., Shi, X., Asiri, A.M., Zhang, Y., Zheng, B., Zhao, H., 2020. P-doped graphene toward enhanced electrocatalytic N2 reduction. Chem. Commun.

Xia, L., Li, B., Zhang, Y., Zhang, R., Ji, L., Chen, H., Cui, G., Zheng, H., Sun, X., Xie, F., 2019. Cr2O3 nanoparticle-reduced graphene oxide hybrid: a highly active electrocatalyst for N2 reduction at ambient conditions. Inorg. Chem. 58, 2257–2260.

Xiong, X., You, C., Liu, Z., Asiri, A.M., Sun, X., 2018. Co-doped CuO nanoarray: an efficient oxygen evolution reaction electrocatalyst with enhanced activity. ACS Sustain. Chem. Eng. 6, 2883–2887.

Xu, D., Zhu, C., Meng, X., Chen, Z., Li, Y., Zhang, D., Zhu, S., 2018. Design and fabrication of Ag-CuO nanoparticles on reduced graphene oxide for nonenzymatic detection of glucose. Sensors Actuators B Chem. 265, 435–442.

Yang, Y., Liu, T., 2011. Fabrication and characterization of graphene oxide/zinc oxide nanorods hybrid. Appl. Surf. Sci. 257, 8950–8954.

Zampardi, G., Thöming, J., Naatz, H., Amin, H.M.A., Pokhrel, S., Mädler, L., Compton, R.G., 2018. Electrochemical behavior of single CuO nanoparticles: implications for the assessment of their environmental fate. Small 14, 1801765.

Zhang, C., Dabbs, D.M., Liu, L.-M., Aksay, I.A., Car, R., Selloni, A., 2015. Combined effects of functional groups, lattice defects, and edges in the infrared spectra of graphene oxide. J. Phys. Chem. C 119, 18167–18176.

Zhang, H., Lv, X., Li, Y., Wang, Y., Li, J., 2010. P25-graphene composite as a high performance photocatalyst. ACS Nano 4, 380–386.

Zhao, C., Lv, J., Xu, X., Zhang, G., Yang, Y., Yang, F., 2017. Highly antifouling and antibacterial performance of poly (vinylidene fluoride) ultrafiltration membranes blending with copper oxide and graphene oxide nanofillers for effective wastewater treatment. J. Colloid Interface Sci. 505, 341–351.

Zhao, Y., Song, X., Song, Q., Yin, Z., 2012. A facile route to the synthesis copper oxide/reduced graphene oxide nanocomposites and electrochemical detection of catechol organic pollutant. CrystEngComm 14, 6710–6719.

Zhu, J., Zeng, G., Nie, F., Xu, X., Chen, S., Han, Q., Wang, X., 2010. Decorating graphene oxide with CuO nanoparticles in a water–isopropanol system. Nanoscale 2, 988–994.